

Kinetic Modulation of Carbon Nanotube Growth in Direct Spinning for High-Strength Carbon Nanotube Fibers

Zuncheng Hu,[†] Xiucan Sun,[†] Xinshi Zhang, Xiangzheng Jia, Xueting Feng, Mingwei Cui, Enlai Gao, Liu Qian,* Xin Gao,* and Jin Zhang*



Cite This: <https://doi.org/10.1021/jacs.4c01705>



Read Online

ACCESS |

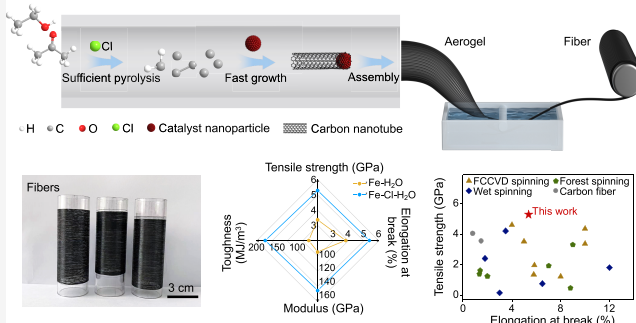
Metrics & More

Article Recommendations

Supporting Information

ABSTRACT: With impressive individual properties, carbon nanotubes (CNTs) show great potential in constructing high-performance fibers. However, the tensile strength of as-prepared carbon nanotube fibers (CNTFs) by floating catalyst chemical vapor deposition (FCCVD) is plagued by the weak intertube interaction between the essential CNTs. Here, we developed a chlorine (Cl)/water (H₂O)-assisted length furtherance FCCVD (CALF-FCCVD) method to modulate the intertube interaction of CNTs and enhance the mechanical strength of macroscopic fibers. The CNTs acquired by the CALF-FCCVD method show an improvement of 731% in length compared to that by the conventional iron-based FCCVD system. Moreover, CNTFs prepared by CALF-FCCVD spinning exhibit a high tensile strength of 5.27 ± 0.27 GPa (4.62 ± 0.24 N/tex) and reach up to 5.61 GPa (4.92 N/tex), which outperforms most previously reported results. Experimental measurements and density functional theory calculations show that Cl and H₂O play a crucial role in the furtherance of CNT growth. Cl released from the decomposition of methylene dichloride greatly accelerates the growth of the CNTs; H₂O can remove amorphous carbon on the floating catalysts to extend their lifetime, which further modulates the growth kinetics and improves the purity of the as-prepared fibers. Our design of the CALF-FCCVD platform offers a powerful way to tune CNT growth kinetics in direct spinning toward high-strength CNTFs.

Cl/H₂O Assisted Length Furtherance Floating Catalyst Chemical Vapor Deposition (CALF-FCCVD)



INTRODUCTION

Carbon nanotubes (CNTs) have received widespread attention from researchers since they were observed in 1991.¹ Along the tube axis, the strong covalent C–C bonds endow CNTs with an ultrahigh elastic modulus (up to 1 TPa)² and tensile strength (up to 100 GPa).³ Benefiting from the unique structure and ultrahigh intrinsic properties, CNTs have been widely considered as an ideal building block to construct fibers with high strength and toughness, which are expected to surpass carbon fibers.⁴ There are three main types of preparation methods of carbon nanotube fibers (CNTFs): wet spinning,⁵ forest spinning,⁶ and floating catalyst chemical vapor deposition (FCCVD) spinning.⁷

Among them, FCCVD can realize continuous production of CNTFs directly after CNT growth and has the potential for large-scale CNTF preparation. In the FCCVD system, the residence time of catalysts in the high-temperature zone is very short (often a few seconds to tens of seconds), and the catalyst is easily poisoned by amorphous carbon coating, which limits the length of CNTs in terms of growth time. Besides, the growth kinetics of CNTs is greatly influenced by the supply rate of active carbon species such as carbon atoms (C)⁸ and carbon dimers (C₂),⁹ which also determines the length of

CNTs in terms of growth rate. Three-level hierarchical model¹⁰ shows the effect of the length of individual CNTs on the mechanical properties of CNTFs. On the one hand, the failure probability of CNTs rises as the length of CNTs increases due to the presence of more defects within longer CNTs. On the other hand, the overlap area between the adjacent CNTs becomes larger with the increasing length of CNTs, which results in enhanced interaction and sufficient load transfer between CNTs. The load transfer plays a leading role in mechanical performance, according to the theoretical model. Therefore, increasing the length of the CNTs in the as-spun CNTFs is an effective way to improve the fiber strength. In addition, although the mechanical properties of CNTFs have been further improved by optimizing spinning and postprocessing technologies on the CNTF level (or CNT bundle level), including adjusting winding rates,¹¹ solvent

Received: February 4, 2024

Revised: March 30, 2024

Accepted: April 1, 2024

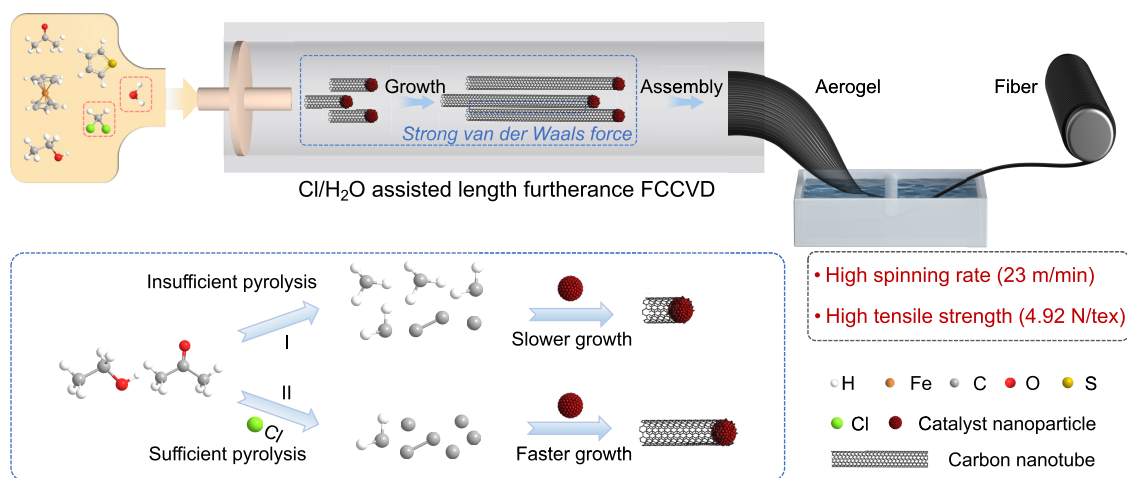


Figure 1. Schematic of high-strength CNTF preparation by the CALF-FCCVD method. Cl/H₂O assisted length furtherance floating catalyst chemical vapor deposition (CALF-FCCVD) process to fast grow long CNTs. A large number of as-prepared CNTs assemble together to obtain high-strength CNTFs. Cl released from CH₂Cl₂ pyrolysis is beneficial for the sufficient pyrolysis of carbon sources, generating more active carbon species (C or C₂) for the growth of CNTs, thereby increasing the growth rate of CNTs. Introducing H₂O avoids the poisoning of catalyst nanoparticles by amorphous carbon, extending the lifetime of the catalysts and increasing the growth time of CNTs.

densification,¹² rolling densification,¹³ acid treatment,^{14,15} and particle beam irradiation,¹⁶ the tensile strength (<5 GPa) of CNTFs by the FCCVD spinning to date has been far below expected due to the friction and slippage between as-grown short CNTs.^{17,18} The length modulation of CNTs in the as-spun CNTFs is the premise for achieving excellent performance. However, studies on the modulation of CNTs in direct spinning are still in their infancy.

Herein, we developed a chlorine (Cl)/ water (H₂O)-assisted length furtherance FCCVD (termed CALF-FCCVD) method to modulate the length of the CNTs and enhance the mechanical strength of macroscopic fibers (Figure 1). Cl released from methylene dichloride (CH₂Cl₂) pyrolysis was introduced into the growth zone to assist the carbon source cracking, generating more C or C₂ species for the growth of CNTs, thus increasing the growth rate of CNTs. A certain amount of H₂O was added to avoid the poisoning of catalyst nanoparticles by amorphous carbon, extending the lifetime of the catalysts and increasing the growth time of the CNTs. By the CALF-FCCVD method, the strength of the as-spun CNTFs reached 1.77 GPa. After chlorosulfonic acid (CSA) stretching and rolling process to increase the orientation and packing density of the CNTFs, their strength reached 5.61 GPa (4.92 N/tex). This work clearly shows that regulating the growth kinetics of CNTs is an important way to prepare high-strength CNTFs.

RESULTS AND DISCUSSION

High-Performance As-Spun CNTFs by the CALF-FCCVD Method. Modulating the composition of the reaction solution is crucial for the continuous collection of high-performance fibers. We performed a modified FCCVD method to directly synthesize high-strength CNTFs (Figure 1) by adding the Cl/H₂O contained precursors. CH₂Cl₂ and H₂O were simultaneously introduced into the precursor solution for the length modulation of CNTs, for the first time. Cl released from the decomposition of CH₂Cl₂ accelerated the pyrolysis of carbon sources and lengthened the growth of as-grown CNTs. H₂O can remove the amorphous carbon covered on the catalyst surface¹⁹ and reduce the weak junction formed by

amorphous carbon to improve the spinning continuity.²⁰ The precursor solution consisting of acetone and ethanol with dissolved ferrocene and thiophene, which acted as carbon sources and catalysts, was injected into the reactor at a rate of 30 mL/h. The reactor furnace was set at 1300 °C and 3000 standard cubic centimeters per minute (sccm) hydrogen, and 2000 sccm argon gas was introduced into the furnace tube. The reactants collide randomly with the gas flow, and CNTs were formed in the high-temperature zone. The as-grown CNTs were assembled into aerogels and were immersed in water for densification to obtain as-spun CNTFs. The molar ratio of Fe to H₂O in the precursor solution was 1:207 for a high-speed continuous spinning. Further, the molar ratio of Fe/Cl was optimized to improve the fiber strength.

Figure 2a and Supplementary Figure 1 show the strength of the as-spun fibers using the CALF-FCCVD method. The CNTFs prepared by the conventional FCCVD method (without Cl-contained precursor) were chosen as the control. The correlation between the strength of CNTFs and the Fe–Cl ratio showed a nonlinear relation. As the Cl content increased, the strength of CNTFs increased and then decreased. The CNTFs of Fe–Cl–H₂O (1:1.6:207) showed the highest strength of 1.77 ± 0.02 GPa, which is a 33% increase in strength compared with the fibers prepared by the conventional FCCVD method (1.33 ± 0.09 GPa).

The inset in Figure 2a shows a digital photograph of the as-spun CNTFs (hundreds of meters) prepared by the CALF-FCCVD method at a high spinning speed of 23 m/min (Supplementary Movie 1). The as-spun CNTFs of Fe–Cl–H₂O (1:1.6:207) exhibit a clean surface with the CNTs tightly intertwining together (Figure 2b,c). The cross-sectional transmission electron microscope (TEM) image shows the fiber consisted of multiwalled CNTs with an average diameter of 9.93 nm (Figure 2d and Supplementary Figure 2). The introduction of Cl did not affect the diameter of the CNTs (Supplementary Figure 2). Figure 2e shows the typical multiwalled CNT connected to a catalyst nanoparticle in the fiber. A high-resolution TEM image of the nanoparticle is shown in Figure 2f (red frame in Supplementary Figure 3). The lattice distance is 0.210 nm, corresponding to the (2 1 1)

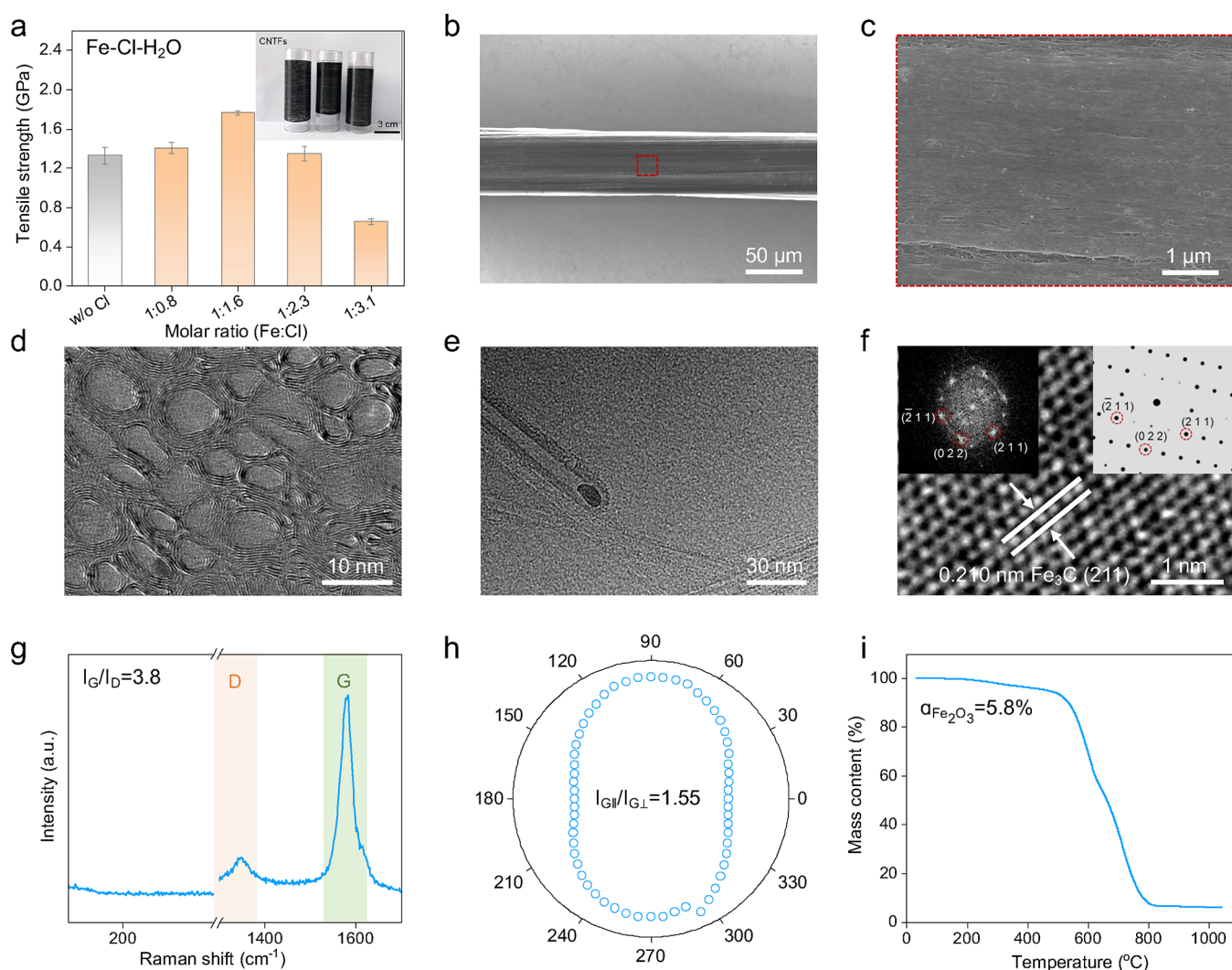


Figure 2. Structure and properties of as-spun CNTFs by the CALF-FCCVD method. (a) On the basis of Fe–H₂O (1:207), the comparison of strength of CNTFs with different contents of Cl. Each bar stands for the mean of replicated tensile strength measurements. Number of replicated measurements (n) is as follows: Fe–H₂O (1:207) ($n = 5$), Fe–Cl–H₂O (1:0.8:207) ($n = 4$), Fe–Cl–H₂O (1:1.6:207) ($n = 5$), Fe–Cl–H₂O (1:2.3:207) ($n = 5$), and Fe–Cl–H₂O (1:3.1:207) ($n = 4$). The inset is a digital photograph of CNTFs. (b) Scanning electron microscope (SEM) image of CNTFs obtained under Fe–Cl–H₂O (1:1.6:207). (c) Zoom-in image of the red frame in panel (b). (d) Cross-sectional TEM image of the CNTFs. (e) TEM image of a CNT connected to a catalyst nanoparticle. (f) High-resolution TEM image of the nanoparticle. Inset: the left panel is the corresponding FFT pattern; the right panel is the simulated diffraction pattern of Fe₃C along the zone axis of [0–1 1]. (g) Raman spectrum, (h) polarized Raman spectrum, and (i) TGA of the CNTFs were obtained under Fe–Cl–H₂O (1:1.6:207).

facet of the iron carbide (Fe₃C) phase.²¹ The fast Fourier transform (FFT) pattern (inset of Figure 2f) agrees perfectly with the simulated diffraction pattern of Fe₃C along the zone axis of [0–1 1].

Figure 2g presents the ratio of the intensity of the G band to that of the D band (I_G/I_D) in the Raman spectra. The D band is related to topological defects and disorders in carbonaceous materials while the G band corresponds to the graphitized carbon. Higher I_G/I_D values indicate a higher quality of CNTs. The CNTFs of Fe–Cl–H₂O (1:1.6:207) show the highest I_G/I_D of 3.8 among all the conditions (Supplementary Figure 4). Cl in the gas phase is beneficial for carbon source cracking. The introduction of an appropriate amount of Cl reduced the amorphous carbon formation. However, excessive Cl will generate excessive carbon species, thus increasing the content of amorphous carbon. Linear density is one of the important physical and geometric characteristics of fibers and describes the thickness of fibers. The linear density of CNTFs increased

with the increase of Cl content (Supplementary Figure 5), further demonstrating that Cl can assist in the cracking of carbon sources. The energy-dispersive X-ray spectroscopy (EDS) shows no signal of Cl in the as-spun fibers (Supplementary Figure 6), which indicates that Cl does not dope the CNTFs.

To characterize the fiber orientation, we used polarized Raman spectroscopy for quantitative analysis.^{15,22} The ratio of the intensity of the G band of the Raman spectrum for the polarization parallel to the fiber axis to that for the polarization perpendicular to the fiber axis ($I_{G||}/I_{G\perp}$) can characterize the orientation of as-prepared fibers. The higher $I_{G||}/I_{G\perp}$ means that the fiber has a higher orientation degree along the axial direction. The CNTFs obtained under Fe–Cl–H₂O (1:1.6:207) show that the $I_{G||}/I_{G\perp}$ value is 1.55 (Figure 2h), which is lower than that ($I_{G||}/I_{G\perp} = 1.85$, Supplementary Figure 7) of Fe–H₂O (1:207). The longer CNTs are easier to entangle together, resulting in a decrease in the orientation

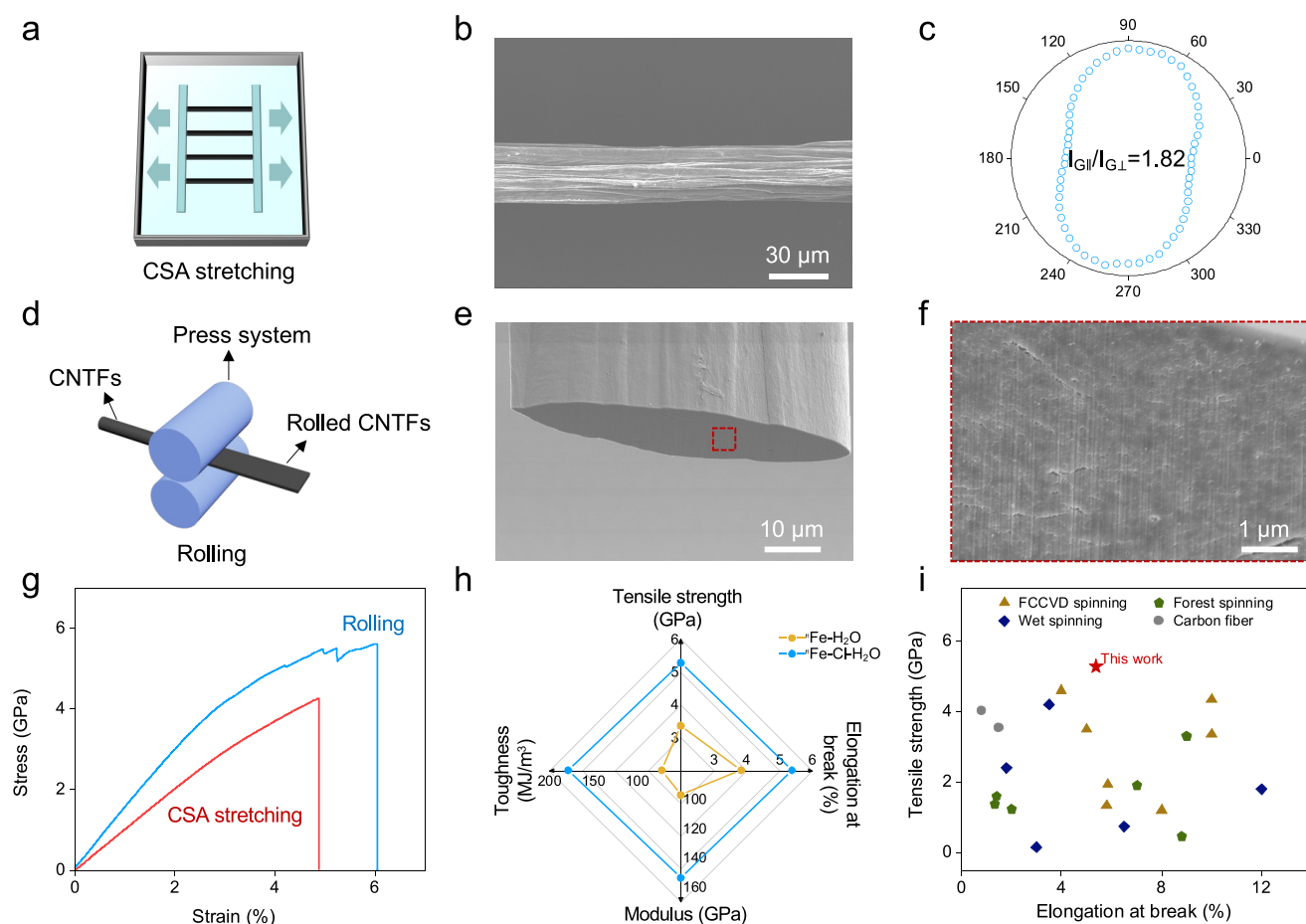


Figure 3. Mechanical properties of CNTFs after post-treatment. (a) Schematic of CSA stretching. (b) SEM image and (c) polarized Raman spectrum of the CNTFs obtained under Fe–Cl–H₂O (1:1.6:207) after CSA stretching. (d) Schematic of rolling. (e) Cross-sectional SEM image of the CNTFs obtained under Fe–Cl–H₂O (1:1.6:207) after rolling. (f) Enlarged image of CNTFs (red frame in panel (e)). (g) Stress–strain curves of CNTFs after CSA stretching and rolling. (h) Comparison of the mechanical properties of CNTFs obtained under Fe–H₂O (1:1:207) and Fe–Cl–H₂O (1:1.6:207). (i) Comparison of tensile strength and elongation at break of our CNTFs with commercial carbon fibers²⁴ and the CNTFs prepared by FCCVD spinning,^{7,11,13,25–28} forest spinning,^{29–34} and wet spinning.^{5,35–38} The exact mechanical performance data for different methods are summarized in [Supplementary Tables 1 and 2](#).

degree. Thermogravimetric analysis (TGA) shows the content of residual Fe₂O₃ in the fiber is as low as 5.8% ([Figure 2i](#)). Assuming all catalysts are oxidized to Fe₂O₃, the residual Fe content is 4.1% ([Supplementary Figure 8b](#)).

Post-Treatment of As-Spun CNTFs. To further improve the mechanical properties of as-spun CNTFs, we densified and aligned the internal structures of CNTFs using CSA stretching and rolling densification. The CSA is known as a thermodynamic solvent for CNT dissolution.²³ Therefore, we first performed CSA stretching ([Figure 3a](#)) on the as-spun CNTFs using the optimal conditions of Fe–Cl–H₂O (1:1.6:207), with a stretching ratio of 5%. [Figure 3b](#) shows the surface morphology of the fiber after stretching. The orientation factor ($I_{G\parallel}/I_{G\perp}$) increases from 1.55 to 1.82 ([Figure 3c](#) and [Supplementary Figure 9c](#)). In addition, the proportion of voids in the cross-section is significantly reduced and the packing density of the fiber is also improved ([Supplementary Figure 10d](#)). Benefiting from the improvement of orientation and packing density, the tensile strength of the fiber was improved to 3.88 ± 0.29 GPa, with a maximum of 4.26 GPa ([Figure 3g](#) and [Supplementary Figure 11b](#)). Moreover, we performed a rolling densification treatment ([Figure 3d](#)) to further compact the CNTFs. The fiber shows a

narrow band shape after rolling ([Figure 3e](#)). Cross-sectional SEM images indicate that CNTs are tightly packed in the fiber ([Figure 3f](#)). After rolling, the mechanical performance was greatly improved compared to the as-spun CNTFs. The tensile strength of the processed fibers is 5.27 ± 0.27 GPa ([Figure 3g](#) and [Supplementary Figure 11d](#)), with a modulus of 153.69 ± 13.86 GPa, a toughness of 178.44 ± 30.31 MJ/m³, and an elongation at break of $5.38 \pm 0.56\%$, displaying 57, 59, 150, and 40% increases compared to CNTFs obtained via the conventional FCCVD method (without Cl precursor) after post-treatment ([Figure 3h](#)). The mechanical performances of as-prepared fibers using the CALF-FCCVD method outperform most previously reported CNTFs ([Figure 3i](#)).

Mechanism for Cl/H₂O-Assisted High-Strength CNTF Preparation. We have developed a three-level hierarchical model¹⁰ to understand the mechanical behavior of CNTFs, which can be used to explain the performance improvement of CNTFs in this work. The introduction of Cl/H₂O increases the length of CNTs by 70–150% compared with the conventional FCCVD method (see [Experimental Section](#) in the Supporting Information for details). This length increase promotes the load transfer efficiency, which helps to improve the mechanical strength of the fibers. However, it should be

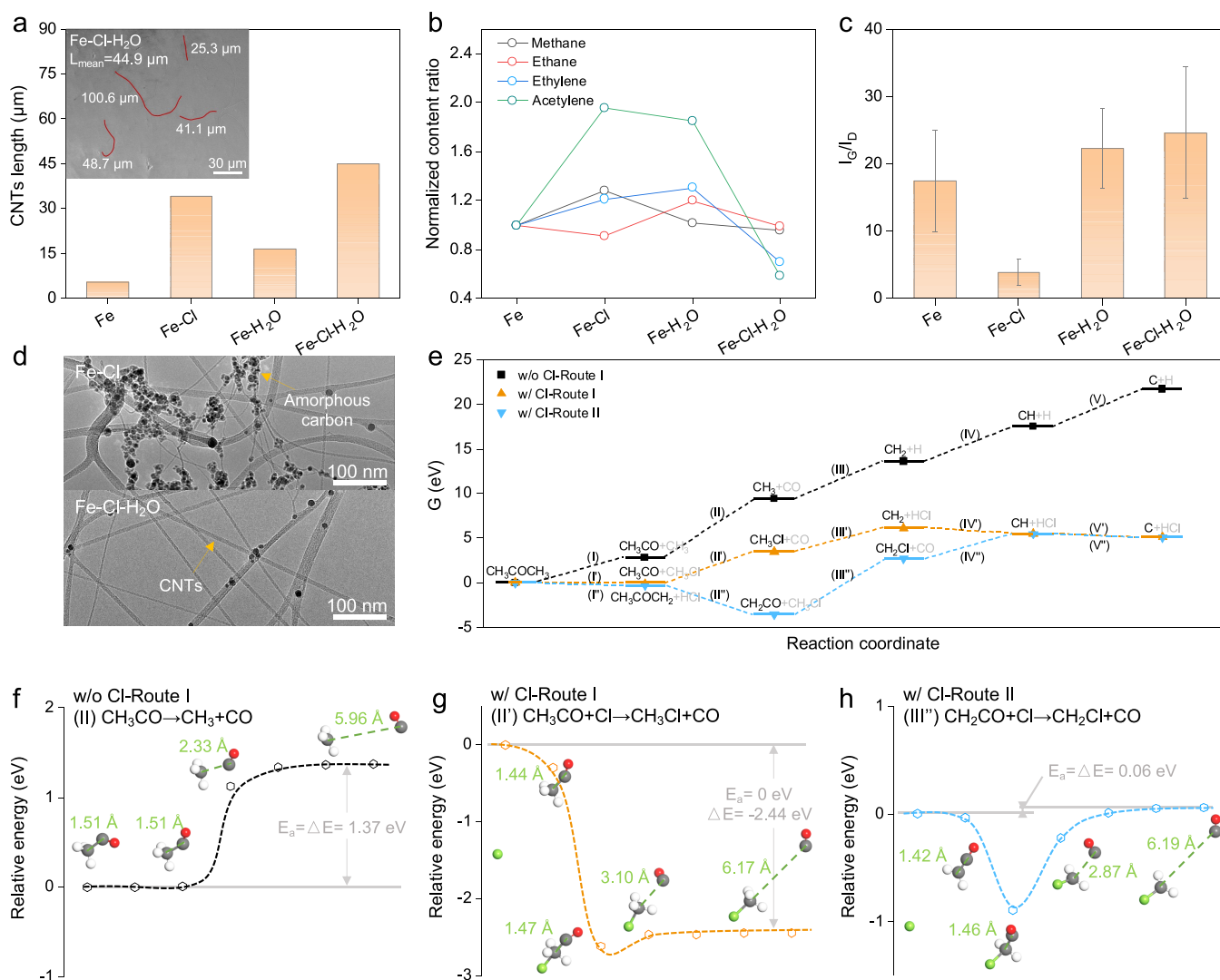


Figure 4. Mechanism analysis for Cl/H₂O-modulated CNT growth. (a) Average CNTs length under different growth conditions. Inset is a typical SEM image of CNTs. The molar ratio of Fe to Cl is 1:2; the molar ratio of Fe to H₂O is 1:2; the molar ratio of Fe to Cl to H₂O is 1:2:2. (b) Normalized contents of CH₄, C₂H₆, C₂H₄, and C₂H₂ in reaction exhaust under different conditions measured by GC-MS. The relative concentration of carbon-containing gas of the reaction exhaust gas indicates the usage of the carbon sources. All values are normalized to those of Fe. (c) I_G/I_D of CNTs under different growth conditions. The number of replicates for each experimental condition is 5. (d) TEM images of as-grown CNTs. (e) Calculated free energy of acetone decomposition with and without Cl. Energy profile of the rate-limiting step in (f) Route I without Cl introduction, (g) Route I with Cl introduction, and (h) Route II with Cl introduction. Compared to the acetone decomposition without Cl introduction, the Cl-modulated reactions have lower ΔG and activation energy (E_a); both factors lead to an elevated concentration of reactive carbon species (C or C₂) and, consequently, fast CNT growth. The green numbers represent the distance between two carbon atoms connected by green dashed line. Green, red, gray, and white spheres are chlorine, oxygen, carbon, and hydrogen atoms, respectively.

noted that accurate characterization of the length of CNTs in these macroscopic CNTFs is challenging due to the entanglement among CNTs.

To visualize the mechanism for Cl/H₂O-assisted long CNTs growth toward high-strength CNTF preparation, we used the horizontal furnace to prepare a small amount of CNTs by the CALF-FCCVD method. The furnace temperature was set at 1100 °C, the injection rate of the catalyst solution was 10 μ L/min, and the total flow rate of argon and hydrogen was 1000 sccm. The conventional FCCVD method without Cl/H₂O precursors was performed for comparison. Four different reaction conditions with different carbon source concentrations (C1–C4, see Experimental Section in the Supporting Information for details) were conducted for CNT growth. The length of as-grown CNTs can be fitted by statistical

distribution and meet the log-normal distribution (Supplementary Figures 12–16). Without Cl and H₂O addition (denoted as Fe; control group), the as-grown CNTs are shorter with length of $5.4 \pm 3.2 \mu\text{m}$ (Supplementary Figure 12). When H₂O was introduced into the precursor solution, the as-grown CNTs became longer and their length increased to $16.6 \pm 13.6 \mu\text{m}$ (Supplementary Figures 15 and 17b), with an average diameter of 1.89 nm (Supplementary Figure 18). Further, we added CH₂Cl₂ to the reaction precursor solutions. The molar ratio of Fe to Cl to H₂O is 1:2:2. CH₂Cl₂ will generate Cl through pyrolysis,³⁹ which can regulate the gas-phase reaction, facilitating the dehydrogenation process of hydrocarbons.⁴⁰ The length of as-grown CNTs is $44.9 \pm 29.3 \mu\text{m}$ (Figure 4a and Supplementary Figure 16b), which shows a

731% increase in length compared with that of the control group ($5.4 \pm 3.2 \mu\text{m}$).

Gas chromatography–mass spectrometry (GC–MS), Raman spectroscopy, and TEM were performed to understand the growth process of CNTs. The carbon-containing gases in the reaction exhaust of conventional Fe catalytic growth system are methane, ethane, ethylene, and acetylene (Supplementary Figure 19 and Supplementary Table 3). With the addition of H_2O , both the concentration of some carbon-containing gases (methane, ethane, ethylene, and acetylene) and the value of I_G/I_D for the as-grown CNTs increased (Figure 4b,c and Supplementary Figures 20 and 21c), which indicated that the increase in CNTs length mainly resulted from the extended catalyst life.⁴¹ When Cl was introduced into the system, the ethane content decreased, while the others increased compared to the control group. Moreover, the I_G/I_D ratio of as-grown CNTs is lower compared with the control group (Figure 4c and Supplementary Figures 20 and 22c). The quality (I_G/I_D) of the product decreases with the increase of Cl content (Supplementary Figure 23). When the Cl content is higher than the threshold (Fe:Cl = 1:8), the product is mainly amorphous carbon (Supplementary Figure 24). Therefore, although the length of CNTs increased after Cl addition, some catalysts were still coated by amorphous carbon and deactivated (Figure 4d). The X-ray photoelectron spectroscopy (XPS) spectrum shows that the CNTs are free of Cl element (Supplementary Figure 25), which implies that Cl works during the growth process. When Cl and H_2O were introduced into the FCCVD system simultaneously, the concentration of some carbon-containing gases (methane, ethane, ethylene, and acetylene) decreased, while the I_G/I_D ratio increased compared with the control group (Figure 4b,c and Supplementary Figures 20 and 26c). The TEM images (Figure 4d) show that the addition of Cl and H_2O leads to less amorphous carbon deposition and improves the purity of the CNTs. Therefore, Cl/ H_2O plays a crucial role in tuning the growth kinetics of CNTs.

To attain an in-depth understanding of the effect of Cl on CNT growth kinetics, we carried out density functional theory (DFT) calculations to simulate the carbon source (acetone and ethanol) decomposition process. According to the overlap populations of chemical bonds (Supplementary Figure 27a), the C–C bond in acetone has the smallest overlap population and the weakest strength, which causes it to break more frequently during gas phase pyrolysis. Subsequently, the hydrocarbon species continue to dehydrogenate in the high-temperature gas phase to provide precursor for the growth of CNTs (following Route I: $\text{CH}_3\text{COCH}_3 \rightarrow \text{CH}_3\text{CO} + \text{CH}_3 \rightarrow \text{CH}_3 + \text{CO} \rightarrow \text{CH}_{3-x} + x\text{H}$), which is consistent with the results of this route (Route I) as the main pathway in the literature⁴² (Supplementary Figure 28). Therefore, we first take the gradual pyrolysis of acetone in Route I as the research object and preliminarily evaluate the influence of Cl through the thermodynamic energy changes of Gibbs free energy (G).

Thermodynamic analysis (Figure 4e and Supplementary Table 4) reveals that the energy gain of gradual pyrolysis of acetone to carbon atoms following Route I is significant, and each acetone molecule needs to absorb 21.70 eV of energy to achieve complete decomposition. Among them, the second step, $\text{CH}_3\text{CO} \rightarrow \text{CH}_3 + \text{CO}$, has the largest free energy increment (ΔG , 6.59 eV), thus serving as a speed limiting step to limit the acetone pyrolysis process. When Cl is introduced into the gas phase, active Cl atoms collide with

acetone molecules to create a connection, which weakens the C–C bonds due to electron relaxation, resulting in the overall ΔG dramatically reduced to 5.11 eV during the full pyrolysis of acetone into carbon atoms. Therefore, the participation of Cl can significantly reduce the reaction heat required for acetone pyrolysis, thereby reducing the difficulty of carbon source pyrolysis. Furthermore, the introduction of Cl also somewhat accelerates the dehydrogenation process of hydrocarbon groups,⁴⁰ which aids in the pyrolysis of acetone along Route II ($\text{CH}_3\text{COCH}_3 \rightarrow \text{CH}_3\text{COCH}_2 + \text{H}$).

From the kinetic perspective, we calculated the activation energy (E_a) of the rate-limiting step for acetone pyrolysis using the nudged elastic band (NEB) method⁴³ to further validate the role of Cl in carbon source pyrolysis. It can be seen that the E_a of the rate-limiting step for direct decomposition of acetone ($\text{CH}_3\text{CO} \rightarrow \text{CH}_3 + \text{CO}$, Figure 4f) is the same as the reaction heat (ΔE , 1.37 eV), indicating that the kinetic decomposition of CH_3CO needs to overcome the energy barrier of 1.37 eV. However, the E_a and ΔE of the $\text{CH}_3\text{CO} + \text{Cl} \rightarrow \text{CH}_3\text{Cl} + \text{CO}$ reaction involving Cl are 0 and -2.44 eV, respectively (Figure 4g). This reaction occurs spontaneously and simultaneously releases 2.44 eV of heat. The rate-limiting step ($\text{CH}_2\text{CO} + \text{Cl} \rightarrow \text{CH}_2\text{Cl} + \text{CO}$) in Route II involving Cl also owns a low E_a of 0.06 eV (Figure 4h). In addition, further calculations showed that the introduction of Cl was also beneficial for the sufficient decomposition of ethanol (Supplementary Figure 29). To further substantiate the mechanism, we performed HCl gas detection for the exhaust gas with and without CH_2Cl_2 . Supplementary Figure 30 and Supplementary Table 5 show the HCl formation after incorporating CH_2Cl_2 , which is consistent with the DFT reaction route with the Cl (Figure 4e). Therefore, introducing CH_2Cl_2 to release Cl in the gas phase can enhance the concentration of activated carbon species (C or C_2) formed by carbon source pyrolysis, enabling fast growth of CNTs.

CONCLUSIONS

In summary, we successfully prepared CNTFs with excellent mechanical properties by the CALF-FCCVD method, achieving a tensile strength of up to 5.61 GPa (4.92 N/tex). Theoretical analysis based on the three-level hierarchical model confirms that we can increase the CNT length and improve CNTF mechanical strength by the CALF-FCCVD method. To investigate the effect of Cl and H_2O on the growth of CNTs, we explored the length modulation of CNTs using a horizontal furnace and achieved a length improvement of 731% by the CALF-FCCVD method. Using DFT calculations, we found that the introduction of Cl is beneficial for the sufficient decomposition of carbon sources in thermodynamics and kinetics to generate sufficient active carbon species (C or C_2), leading to the fast growth of CNTs. Besides, the introduction of H_2O is beneficial for the increase in catalyst lifetime. These two factors contribute to improving the utilization of carbon sources during the growth process of CNTs, achieving the preparation of long CNTs. Our study provides a method to optimize the strength of macro CNTFs by modulating the properties of micro constituent CNTs in direct spinning.

ASSOCIATED CONTENT

Supporting Information

The Supporting Information is available free of charge at <https://pubs.acs.org/doi/10.1021/jacs.4c01705>.

Details about the experimental and computational methods, statistics of CNT length and diameter, linear density and orientation of CNTFs, GC–MS analysis, and mechanical performance (PDF)

As-spun CNTFs prepared by the CALF-FCCVD method (MP4)

AUTHOR INFORMATION

Corresponding Authors

Liu Qian – School of Materials Science and Engineering, Peking University, Beijing 100871, China; Email: qianliu-cnc@pku.edu.cn

Xin Gao – School of Materials Science and Engineering, Peking University, Beijing 100871, China; Beijing Graphene Institute (BGI), Beijing 100095, China; orcid.org/0000-0001-5360-0796; Email: gaoxin-cnc@pku.edu.cn

Jin Zhang – Center for Nanochemistry, Beijing Science and Engineering Center for Nanocarbons, Beijing National Laboratory for Molecular Sciences, College of Chemistry and Molecular Engineering and School of Materials Science and Engineering, Peking University, Beijing 100871, China; Beijing Graphene Institute (BGI), Beijing 100095, China; orcid.org/0000-0003-3731-8859; Email: jinzhang@pku.edu.cn

Authors

Zuncheng Hu – Center for Nanochemistry, Beijing Science and Engineering Center for Nanocarbons, Beijing National Laboratory for Molecular Sciences, College of Chemistry and Molecular Engineering and School of Materials Science and Engineering, Peking University, Beijing 100871, China

Xiucui Sun – Beijing Graphene Institute (BGI), Beijing 100095, China

Xinshi Zhang – Center for Nanochemistry, Beijing Science and Engineering Center for Nanocarbons, Beijing National Laboratory for Molecular Sciences, College of Chemistry and Molecular Engineering and School of Materials Science and Engineering, Peking University, Beijing 100871, China; Beijing Graphene Institute (BGI), Beijing 100095, China

Xiangzheng Jia – Department of Engineering Mechanics, School of Civil Engineering, Wuhan University, Wuhan 430072, China

Xueting Feng – Center for Nanochemistry, Beijing Science and Engineering Center for Nanocarbons, Beijing National Laboratory for Molecular Sciences, College of Chemistry and Molecular Engineering, Peking University, Beijing 100871, China

Mingwei Cui – Center for Nanochemistry, Beijing Science and Engineering Center for Nanocarbons, Beijing National Laboratory for Molecular Sciences, College of Chemistry and Molecular Engineering and School of Materials Science and Engineering, Peking University, Beijing 100871, China

Enlai Gao – Department of Engineering Mechanics, School of Civil Engineering, Wuhan University, Wuhan 430072, China; orcid.org/0000-0003-1960-0260

Complete contact information is available at:

<https://pubs.acs.org/10.1021/jacs.4c01705>

Author Contributions

[†]Z.H. and X.S. contributed equally to this work.

Notes

The authors declare no competing financial interest.

ACKNOWLEDGMENTS

We thank Suzhou Institute of Nano-Tech and Nano-Bionics, Chinese Academy of Sciences for fiber preparation support. This work was supported by the Ministry of Science and Technology of China (2022YFA1203302, 2022YFA1203304, and 2018YFA0703502), the National Natural Science Foundation of China (grant nos. 52021006, 52102032), the Strategic Priority Research Program of CAS (XDB36030100), and the Beijing National Laboratory for Molecular Sciences (BNLMS-CXTD-202001). X.G. thanks the National Natural Science Foundation of China (grant no. 52302034). The numerical calculations in this work were done on the supercomputing system in the Supercomputing Center of Wuhan University.

REFERENCES

- (1) Iijima, S. Helical microtubules of graphitic carbon. *Nature* **1991**, *354* (6348), 56–58.
- (2) Zhang, R. F.; Wen, Q.; Qian, W. Z.; Su, D. S.; Zhang, Q.; Wei, F. Superstrong ultra long carbon nanotubes for mechanical energy storage. *Adv. Mater.* **2011**, *23* (30), 3387–3391.
- (3) Peng, B.; Locascio, M.; Zapol, P.; Li, S. Y.; Mielke, S. L.; Schatz, G. C.; Espinosa, H. D. Measurements of near-ultimate strength for multiwalled carbon nanotubes and irradiation-induced crosslinking improvements. *Nat. Nanotechnol.* **2008**, *3* (10), 626–631.
- (4) Wu, Y. Z.; Zhao, X. W.; Shang, Y. Y.; Chang, S. L.; Dai, L. X.; Cao, A. Y. Application-driven carbon nanotube functional materials. *ACS Nano* **2021**, *15* (5), 7946–7974.
- (5) Vigolo, B.; Penicaud, A.; Coulon, C.; Sauder, C.; Pailler, R.; Journet, C.; Bernier, P.; Poulin, P. Macroscopic fibers and ribbons of oriented carbon nanotubes. *Science* **2000**, *290* (5495), 1331–1334.
- (6) Jiang, K. L.; Li, Q. Q.; Fan, S. S. Nanotechnology: Spinning continuous carbon nanotube yarns - Carbon nanotubes weave their way into a range of imaginative macroscopic applications. *Nature* **2002**, *419* (6909), 801–801.
- (7) Zhu, H. W.; Xu, C. L.; Wu, D. H.; Wei, B. Q.; Vajtai, R.; Ajayan, P. M. Direct synthesis of long single-walled carbon nanotube strands. *Science* **2002**, *296* (5569), 884–886.
- (8) Ding, F.; Bolton, K.; Rosen, A. Nucleation and growth of single-walled carbon nanotubes: A molecular dynamics study. *J. Phys. Chem. B* **2004**, *108* (45), 17369–17377.
- (9) Rao, R.; Liptak, D.; Cherukuri, T.; Yakobson, B. I.; Maruyama, B. In situ evidence for chirality-dependent growth rates of individual carbon nanotubes. *Nat. Mater.* **2012**, *11* (3), 213–216.
- (10) Gao, E. L.; Lu, W. B.; Xu, Z. P. Strength loss of carbon nanotube fibers explained in a three-level hierarchical model. *Carbon* **2018**, *138*, 134–142.
- (11) Zhou, T.; Niu, Y. T.; Li, Z.; Li, H. F.; Yong, Z. Z.; Wu, K. J.; Zhang, Y. Y.; Li, Q. W. The synergetic relationship between the length and orientation of carbon nanotubes in direct spinning of high-strength carbon nanotube fibers. *Mater. Des.* **2021**, *203*, No. 109557.
- (12) Zhong, X. H.; Li, Y. L.; Liu, Y. K.; Qiao, X. H.; Feng, Y.; Liang, J.; Jin, J.; Zhu, L.; Hou, F.; Li, J. Y. Continuous multilayered carbon nanotube yarns. *Adv. Mater.* **2010**, *22* (6), 692–696.
- (13) Wang, J. N.; Luo, X. G.; Wu, T.; Chen, Y. High-strength carbon nanotube fibre-like ribbon with high ductility and high electrical conductivity. *Nat. Commun.* **2014**, *5* (1), 3848.
- (14) Wang, J. J.; Zhao, J. N.; Zhao, L. M.; Lu, Q.; Zhou, T.; Yong, Z. Z.; Wang, P. F.; Zhang, X. H.; Li, Q. W. Interfacial-bubbling-induced nondestructive expansion to reconstruct superstrong and multifunctional carbon nanotube fibers. *Carbon* **2021**, *184*, 24–33.
- (15) Lee, J.; Lee, D.-M.; Jung, Y.; Park, J.; Lee, H. S.; Kim, Y.-K.; Park, C. R.; Jeong, H. S.; Kim, S. M. Direct spinning and densification method for high-performance carbon nanotube fibers. *Nat. Commun.* **2019**, *10* (1), 2962.
- (16) Miao, M. H.; Hawkins, S. C.; Cai, J. Y.; Gengenbach, T. R.; Knott, R.; Huynh, C. P. Effect of gamma-irradiation on the

- mechanical properties of carbon nanotube yarns. *Carbon* **2011**, *49* (14), 4940–4947.
- (17) Wen, Y. Y.; Jian, M. Q.; Huang, J. K.; Luo, J. J.; Qian, L.; Zhang, J. Carbonene fibers: Toward next-generation fiber materials. *Nano Lett.* **2022**, *22* (15), 6035–6047.
- (18) Ma, W. J.; Liu, L. Q.; Yang, R.; Zhang, T. H.; Zhang, Z.; Song, L.; Ren, Y.; Shen, J.; Niu, Z. Q.; Zhou, W. Y.; Xie, S. S. Monitoring a micromechanical process in macroscale carbon nanotube films and fibers. *Adv. Mater.* **2009**, *21* (5), 603–608.
- (19) Yamada, T.; Maigne, A.; Yudasaka, M.; Mizuno, K.; Futaba, D. N.; Yumura, M.; Iijima, S.; Hata, K. Revealing the secret of water-assisted carbon nanotube synthesis by microscopic observation of the interaction of water on the catalysts. *Nano Lett.* **2008**, *8* (12), 4288–4292.
- (20) Dong, L. Y.; Park, J. G.; Leonhardt, B. E.; Zhang, S. L.; Liang, R. Continuous synthesis of double-walled carbon nanotubes with water-assisted floating catalyst chemical vapor deposition. *Nanomaterials* **2020**, *10* (2), 365.
- (21) Yang, W. X.; Liu, X. J.; Yue, X. Y.; Jia, J. B.; Guo, S. J. Bamboo-like carbon nanotube/Fe₃C nanoparticle hybrids and their highly efficient catalysis for oxygen reduction. *J. Am. Chem. Soc.* **2015**, *137* (4), 1436–1439.
- (22) Gommans, H. H.; Alldredge, J. W.; Tashiro, H.; Park, J.; Magnuson, J.; Rinzler, A. G. Fibers of aligned single-walled carbon nanotubes: Polarized Raman spectroscopy. *J. Appl. Phys.* **2000**, *88* (5), 2509–2514.
- (23) Davis, V. A.; Parra-Vasquez, A. N. G.; Green, M. J.; Rai, P. K.; Behabtu, N.; Prieto, V.; Booker, R. D.; Schmidt, J.; Kesselman, E.; Zhou, W.; Fan, H.; Adams, W. W.; Hauge, R. H.; Fischer, J. E.; Cohen, Y.; Talmon, Y.; Smalley, R. E.; Pasquali, M. True solutions of single-walled carbon nanotubes for assembly into macroscopic materials. *Nat. Nanotechnol.* **2009**, *4* (12), 830–834.
- (24) Liu, Y. D.; Kumar, S. Recent progress in fabrication, structure, and properties of carbon fibers. *Polym. Rev.* **2012**, *52* (3), 234–258.
- (25) Liu, F.; Wang, Q.; Zhai, G.; Xiang, H.; Zhou, J.; Jia, C.; Zhu, L.; Wu, Q.; Zhu, M. Continuously processing waste lignin into high-value carbon nanotube fibers. *Nat. Commun.* **2022**, *13* (1), 5755.
- (26) Shang, Y. Y.; Wang, Y.; Li, S. H.; Hua, C. F.; Zou, M. C.; Cao, A. Y. High-strength carbon nanotube fibers by twist-induced self-strengthening. *Carbon* **2017**, *119*, 47–55.
- (27) Zhang, X.; De Volder, M.; Zhou, W.; Issman, L.; Wei, X.; Kaniyoor, A.; Portas, J. T.; Smail, F.; Wang, Z.; Wang, Y.; Liu, H.; Zhou, W.; Elliott, J.; Xie, S.; Boies, A. Simultaneously enhanced tenacity, rupture work, and thermal conductivity of carbon nanotube fibers by raising effective tube portion. *Sci. Adv.* **2022**, *8* (50), No. eabq3515.
- (28) Cho, Y. S.; Lee, J. W.; Kim, J.; Jung, Y.; Yang, S. J.; Park, C. R. Superstrong carbon nanotube yarns by developing multiscale bundle structures on the direct spin-line without post-treatment. *Adv. Sci.* **2023**, *10* (2), No. 2204250.
- (29) Kinoshita, T.; Karita, M.; Chikyu, N.; Nakano, T.; Inoue, Y. Enhancement of catalytic activity by addition of chlorine in chemical vapor deposition growth of carbon nanotube forests. *Carbon* **2022**, *196*, 391–400.
- (30) Zhang, M.; Atkinson, K. R.; Baughman, R. H. Multifunctional carbon nanotube yarns by downsizing an ancient technology. *Science* **2004**, *306* (5700), 1358–1361.
- (31) Zhang, X. F.; Li, Q. W.; Holesinger, T. G.; Arendt, P. N.; Huang, J. Y.; Kirven, P. D.; Clapp, T. G.; DePaula, R. F.; Liao, X. Z.; Zhao, Y. H.; Zheng, L. X.; Peterson, D. E.; Zhu, Y. T. Ultrastrong, stiff, and lightweight carbon-nanotube fibers. *Adv. Mater.* **2007**, *19* (23), 4198–4201.
- (32) Jia, J. J.; Zhao, J. N.; Xu, G.; Di, J. T.; Yong, Z. Z.; Tao, Y. Y.; Fang, C. O.; Zhang, Z. G.; Zhang, X. H.; Zheng, L. X.; Li, Q. W. A comparison of the mechanical properties of fibers spun from different carbon nanotubes. *Carbon* **2011**, *49* (4), 1333–1339.
- (33) Zhang, X. F.; Li, Q. W.; Tu, Y.; Li, Y. A.; Coulter, J. Y.; Zheng, L. X.; Zhao, Y. H.; Jia, Q. X.; Peterson, D. E.; Zhu, Y. T. Strong carbon-nanotube fibers spun from long carbon-nanotube arrays. *Small* **2007**, *3* (2), 244–248.
- (34) Liu, K.; Zhu, F.; Liu, L.; Sun, Y. H.; Fan, S. S.; Jiang, K. L. Fabrication and processing of high-strength densely packed carbon nanotube yarns without solution processes. *Nanoscale* **2012**, *4* (11), 3389–3393.
- (35) Miaudet, P.; Badaire, S.; Maugey, M.; Derre, A.; Pichot, V.; Launois, P.; Poulin, P.; Zakri, C. Hot-drawing of single and multiwalled carbon nanotube fibers for high toughness and alignment. *Nano Lett.* **2005**, *5* (11), 2212–2215.
- (36) Taylor, L. W.; Dewey, O. S.; Headrick, R. J.; Komatsu, N.; Peraca, N. M.; Wehmeyer, G.; Kono, J.; Pasquali, M. Improved properties, increased production, and the path to broad adoption of carbon nanotube fibers. *Carbon* **2021**, *171*, 689–694.
- (37) Tsentelovich, D. E.; Headrick, R. J.; Mirri, F.; Hao, J. L.; Behabtu, N.; Young, C. C.; Pasquali, M. Influence of carbon nanotube characteristics on macroscopic fiber properties. *ACS Appl. Mater. Interfaces* **2017**, *9* (41), 36189–36198.
- (38) Jiao, X. Y.; Shi, C.; Zhao, Y. M.; Xu, L. L.; Liu, S. K.; Hou, P. X.; Liu, C.; Cheng, H. M. Efficient fabrication of high-quality single-walled carbon nanotubes and their macroscopic conductive fibers. *ACS Nano* **2022**, *16* (12), 20263–20271.
- (39) Wu, Y. P.; Won, Y. S. Pyrolysis of chloromethanes. *Combust. Flame* **2000**, *122* (3), 312–326.
- (40) Xu, S.; Cheng, T.; Yan, Q.; Shen, C.; Yu, Y.; Lin, C.-T.; Ding, F.; Zhang, J. Chloroform-assisted rapid growth of vertical graphene array and its application in thermal interface materials. *Adv. Sci.* **2022**, *9* (15), No. 2200737.
- (41) Hata, K.; Futaba, D. N.; Mizuno, K.; Namai, T.; Yumura, M.; Iijima, S. Water-assisted highly efficient synthesis of impurity-free single-walled carbon nanotubes. *Science* **2004**, *306* (5700), 1362–1364.
- (42) Zaleski, D. P.; Sivaramakrishnan, R.; Weller, H. R.; Seifert, N. A.; Bross, D. H.; Ruscic, B.; Moore, K. B.; Elliott, S. N.; Copan, A. V.; Harding, L. B.; Klippenstein, S. J.; Field, R. W.; Prozument, K. Substitution reactions in the pyrolysis of acetone revealed through a modeling, experiment, theory paradigm. *J. Am. Chem. Soc.* **2021**, *143* (8), 3124–3142.
- (43) Mills, G.; Jonsson, H.; Schenter, G. K. Reversible work transition state theory: application to dissociative adsorption of hydrogen. *Surf. Sci.* **1995**, *324* (2–3), 305–337.